Chinese Chemical Letters 36 (2025) 110177

Contents lists available at ScienceDirect

Chinese Chemical Letters

journal homepage: www.elsevier.com/locate/cclet

Thickness-controllable synthesis of metal-organic framework based hollow nanoflowers with magnetic core *via* liquid phase epitaxy for phosphopeptides enrichment

Ning Zhang[a,*], Mengjie Qin[a], Jiawen Zhu[a], Xuejing Lou[a], Xiao Tian[a], Wende Ma[c], Youmei Wang[a], Minghua Lu[a,*], Zongwei Cai[b,*]

[a] College of Chemistry and Molecular Sciences, Henan University, Kaifeng 475004, China
[b] State Key Laboratory of Environmental and Biological Analysis, Department of Chemistry, Hong Kong Baptist University, Hong Kong, China
[c] State Key Laboratory of Environmental Chemistry and Ecotoxicology, Research Center for Eco-Environmental Sciences, Chinese Academy of Sciences, Beijing 100085, China

ARTICLE INFO

Article history:
Received 28 January 2024
Revised 9 June 2024
Accepted 25 June 2024
Available online 25 June 2024

Keywords:
Metal-organic framework
Nanoflower
Phosphopeptide
Serum
Saliva

ABSTRACT

A thickness-controllable method for preparing metal-organic framework hollow nanoflowers on magnetic cores (Fe_3O_4@MOFs HFs) was demonstrated for the first time. The petal of magnetic core with hollow nanoflower structure served as medium for assembling UiO-66-NH_2 shell with different thickness. To further improve its performance, Zr^{4+} was immobilized on the surface of Fe_3O_4@UiO-66-NH_2. Compared with conventional Fe_3O_4@UiO-66-NH_2-Zr^{4+} nanospheres, the Fe_3O_4@UiO-66-NH_2-Zr^{4+} HFs showed increased enrichment performance for phosphopeptides. The Fe_3O_4@UiO-66-NH_2-Zr^{4+} HFs served as an attractive restricted-access adsorption material exhibited good selectivity ($m_{\beta\text{-casein}}$:m_{BSA}=1:1000), high sensitivity (1.0 fmol) and excellent size-exclusion effect ($m_{\beta\text{-casein digests}}$:$m_{BSA}$=1:200). Furthermore, the Fe_3O_4@UiO-66-NH_2-Zr^{4+} HFs was successfully applied to the specific capture of ultratrace phosphopeptide from complex biological samples, revealing the great potential for the identification and analysis of trace phosphopeptides in clinical analysis. This work can be easily extended to the fabrication of diverse mag-MOF HFs with multifunctional and easy to post-modify properties, and open up a new avenue for the design and construction of new MOFs material.

Heterogeneous nanomaterials are considered as one of the most important candidates in widespread applications [1-5]. Considerable attention has been focused on the heterostructure from porous organic framework materials to prepare alloyed, doped, or hybrid nanomaterials for enhanced adsorption or selective performance [6-8]. Metal organic frameworks (MOFs) are connected *via* organic linkers and metal ions/clusters to form porous frameworks, and have attracted much attention [9-11]. MOFs provide an extensive combination of building units (inorganic nodes and organic linkers) to achieve desired structures and functionalities [12]. Therefore, many efforts have been devoted to prepare MOF-based heterogeneous nanomaterials for enhancing the monomeric performance. Regardless of doping any materials, the new structures and novel properties are generated in the hybrid heterogeneous nanomaterials [13-16]. A growing number of hybrid MOF-based heterogeneous nanomaterials have been prepared and used in various fields.

Previous studies on hybrid MOF-based heterogeneous nanomaterials mainly focused on relatively single core-shell shape, which leaded to the inability to maximize properties of heterogeneous structures [2,4,17,18]. As one of the most important parameters, the shape of materials usually has significant effect on their performance. The hollow MOFs were successfully fabricated and showed boosted surface area, superb porosity, and excellent pore accessibility, and exhibited a significantly improved performance [19]. Wang *et al.* reported the dendritic Ag nanocrystals mimicking the structural feature (dendritic) of moth's antennae. The existence of numerous cavity traps in Ag dendritic nanocrystals prolonged reaction time of the gaseous molecules on the surface of solid surface through the "cavity-vortex" effect bring the more sensitive detection sensitivity [20]. A large number of works have verified the positive influence of the shape on material performance [19-22]. But, no works has thus far paid close attention in heteroge-

* Corresponding authors.
E-mail addresses: zn@henu.edu.cn (N. Zhang), mhlu@henu.edu.cn (M. Lu), zwcai@hkbu.edu.hk (Z. Cai).

https://doi.org/10.1016/j.cclet.2024.110177
1001-8417/

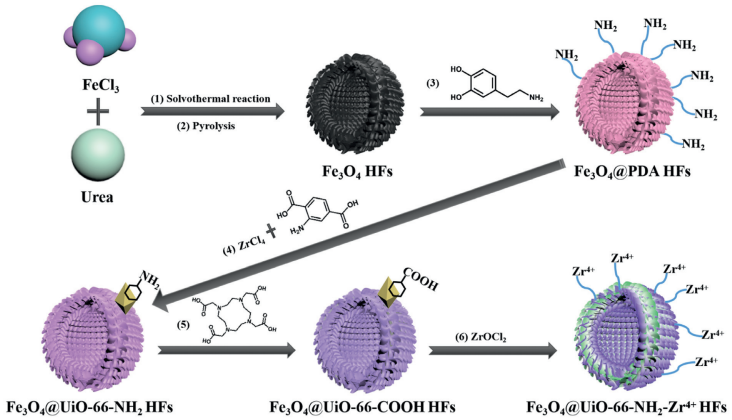

Scheme 1. The formation processes of Fe_3O_4@UiO-66-NH_2-Zr^{4+} HFs.

neous nanomaterials with the special shapes, which hindered the exploration of controllable design of novel heterogeneous materials complexes.

Thus, the aim of this work is to provide a viable and versatile strategy for preparing thickness-controllable MOF based hollow nanoflowers with magnetic core (Fe_3O_4@MOFs HFs). Here, the magnetic core hollow nanoflowers (Fe_3O_4 HFs) were firstly synthesizeds. The Fe_3O_4 HFs were employed as the core, metal organic frameworks shell with magnetic core (Fe_3O_4@MOFs HFs) was prepared by liquid phase epitaxy. The thickness of the MOFs shell was randomly controlled by changing the period of assembly. To achieve higher performance, Fe_3O_4@UiO-66-NH_2 HFs were post-modified with Zr^{4+} ion to generate Fe_3O_4@UiO-66-NH_2-Zr^{4+} HFs, which was successfully used to separate and enrich low-abundance phosphopeptides from complex biological samples. This work provides a new avenue for the design and construction of hybrid MOF-based heterogeneous nanomaterials with hollow nanoflower morphology.

The schematic design of the Fe_3O_4@UiO-66-NH_2-Zr^{4+} HFs was shown in Scheme 1. Firstly, the precursor hollow nanoflowers (PC HFs) were obtained by the solvothermal reaction with $FeCl_3$ and urea, and then transformed into Fe_3O_4 HFs after calcination. The polydopamine (PDA) was modified on the surface of Fe_3O_4 HFs, and the NH_2 groups of PDA could react with metal ions (Fe_3O_4@PDA HFs). Then, Fe_3O_4@UiO-66-NH_2 HFs was prepared by the assembling of Fe_3O_4@PDA HFs and MOF stock solution. Finally, the MOF surface was functionalized by -COOH, and Zr^{4+} was then immobilized on the material by -COOH. During the process of Zr^{4+} immobilization, the coordination interaction between -COOH group and Zr^{4+} served as the driving force. Surprisingly, the thickness of the MOFs shell could be controlled by changing the period of assembly.

The structures and morphologies of the prepared materials were thoroughly characterized by scanning electron microscopy (SEM) and transmission electron microscopy (TEM). It was clear that the hollow nanoflowers was organized from nanosheets as building blocks (Figs. 1A, E and I). After a mild heat-treatment was applied on PC HFs, the Fe_3O_4 with thinner and folded nanosheets was obtained (Figs. 1B, F and J). After stirring with PDA, the edges of magnetic nanoflowers were wrapped by the thin layers, which indicated that the PDA was firmly covered on the surface of Fe_3O_4 HFs (Figs. 1C, G and K). The surface of nanopetals were then assembled by a layer of MOF after heated with MOF stock solution for a period of time (Figs. 1D, H and L). From Fig. 1D and Fig. S1 (Supporting information), as the increase of assembly cycles, the thickness of the nanosheets increased until the space between the petals were fully filled up, and then a pure MOF shells were

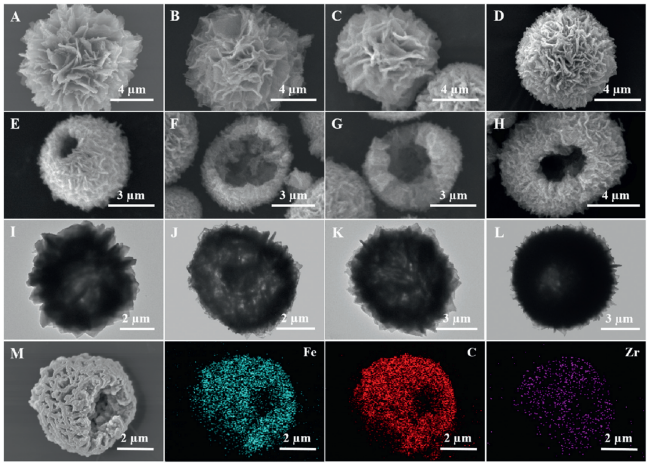

Fig. 1. SEM images of the PC HFs (A), Fe_3O_4 HFs (B), Fe_3O_4@PDA HFs (C), Fe_3O_4@UiO-66-NH_2 HFs (D) with different magnifications. SEM and TEM images for inner hollow structure of PC HFs (E, I), Fe_3O_4 HFs (F, J), Fe_3O_4@PDA HFs (G, K), Fe_3O_4@UiO-66-NH_2 HFs (H, L). (M) Elemental mapping of the Fe_3O_4@UiO-66-NH_2 HFs.

formed on the surface of Fe_3O_4 HFs. Comparing Fig. 1C and Fig. S1A, after one cycle, the thickness of the MOF layer was approximately 80 nm. After another cycle, the thickness of the MOF layer further increased by approximately 163 nm (Fig. S1B). The material that had undergone 5 cycles was completely covered by MOF layer (Figs. S1C and D). Furthermore, the distributions of elements from the area mapping showed a uniform distribution of the metallic distribution of Fe, C and Zr in the Fe_3O_4@UiO-66-NH_2 HFs, which highly indicated that the UiO-66-NH_2 nanoparticles were formed on the surface of Fe_3O_4 HFs and the Fe_3O_4@UiO-66-NH_2 products still kept the hollow structure (Fig. 1M).

Fourier transform infrared spectra (FT-IR) of materials were presented in Fig. 2A. Compared with PC, other HFs materials possessed the characteristic peaks (546 cm^{-1}) belonging to Fe-O [23]. Compared with Fe_3O_4 HFs, the new peak appeared at around 1490 cm^{-1} in Fe_3O_4@PDA HFs, which attributed to the aromatic rings of PDA shell [24]. The FT-IR spectrum of Fe_3O_4@UiO-66-NH_2 obtained after the assembling between the Fe_3O_4@PDA HFs and reaction solution of UiO-66-NH_2. The characteristic peaks appeared at 1651, 1559, 1434, 1385 cm^{-1} could be ascribed to carboxyl groups stretching modes in the Fe_3O_4@UiO-66-NH_2 [25]. The absorption bands of 1250 and 764 cm^{-1} were referred to the C–N and N–H stretching bands in the 2-aminoterephthalic acid, confirming the existence of –NH_2 groups [26].

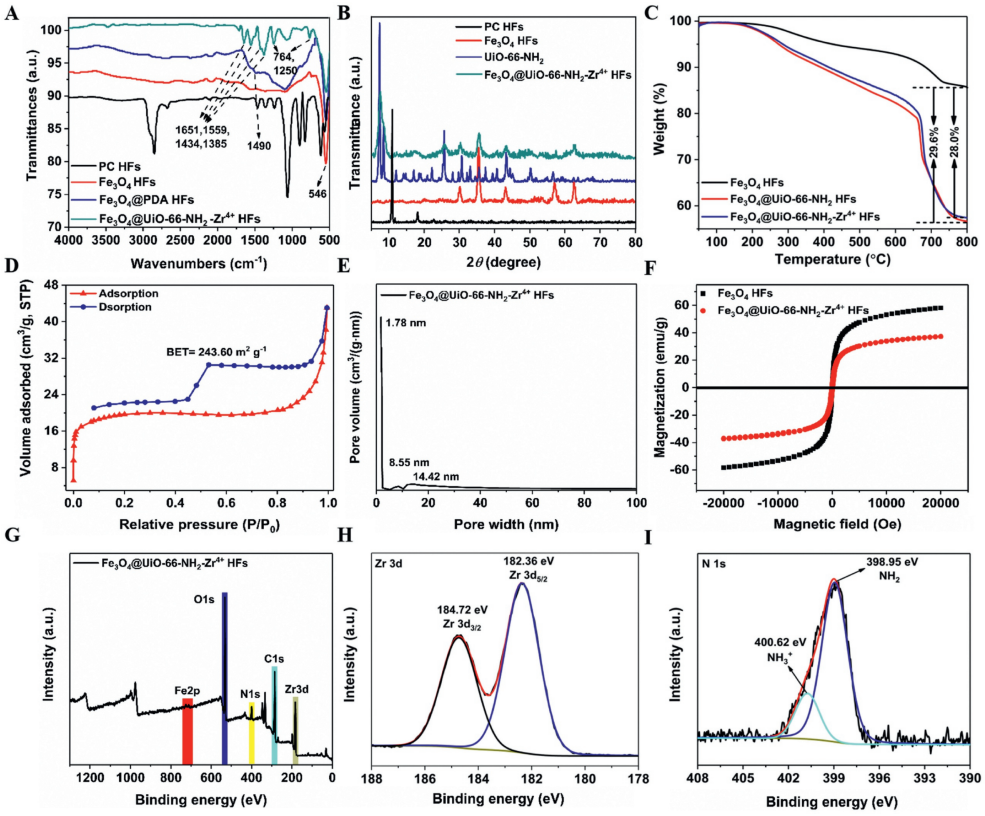

Fig. 2. (A) FTIR spectra of PC, Fe_3O_4, Fe_3O_4@PDA, Fe_3O_4@UiO-66-NH_2. (B) XRD patterns of PC, Fe_3O_4, UiO-66-NH_2, Fe_3O_4@UiO-66-NH_2-Zr^{4+}. (C) TGA curves of Fe_3O_4, Fe_3O_4@UiO-66-NH_2, Fe_3O_4@UiO-66-NH_2-Zr^{4+}. Nitrogen adsorption/desorption isotherms (D) and pore radial distribution (E) of Fe_3O_4@UiO-66-NH_2-Zr^{4+}. (F) Magnetic curves of Fe_3O_4 HFs and Fe_3O_4@UiO-66-NH_2-Zr^{4+}. XPS spectra of Fe_3O_4@UiO-66-NH_2-Zr^{4+} HFs (G), Zr 3d (H) and N 1s (I).

In order to further verify the existence of MOF shell and whether post-modification would affect the crystallinity of MOF, X-ray diffractometer (XRD) of PC, Fe_3O_4, UiO-66-NH_2 and Fe_3O_4@UiO-66-NH_2-Zr^{4+} HFs were further studied. Compared the spectra of PC and Fe_3O_4 in Fig. 2B, the typical diffraction peaks of Fe_3O_4 (30.2° (220), 35.3° (311), 43.3° (400), 57.1° (511), 62.6° (440)) appeared newly in the Fe_3O_4 spectrum, which indicated the properties of nanomaterials were changed from non-magnetic to magnetic during the high-temperature calcination process. From the spectra of Fe_3O_4, UiO-66-NH_2 and Fe_3O_4@UiO-66-NH_2-Zr^{4+} HFs, the additional new diffraction peaks at around 7.5° and 25.8° could be assigned to the crystalline structure of the MOFs (UiO-66-NH_2).

To examine the structural formation, the thermal gravimetric analyser (TGA) of materials were studied (Fig. 2C). Compared with Fe_3O_4, the Fe_3O_4@UiO-66-NH_2 HFs showed extra weight loss of almost 28.0%, indicating that the MOF shell was high yielding. Meanwhile, the TGA analysis of the Fe_3O_4@UiO-66-NH_2-Zr^{4+} HFs showed the extra weight loss which up to 29.6% compared with the Fe_3O_4. The calculated weight loss of 1.6% was attributed to the post-synthetic modifications of Zr^{4+}, also indicating that the Zr^{4+} groups was high yielding. The large loading yields of MOF and Zr^{4+} would help increase performance of the as-prepared materials. The surface area and pore structure were investigated. As shown in Fig. 2D, the Fe_3O_4@UiO-66-NH_2-Zr^{4+} HFs composites displayed typical IV sorption isotherm profiles with the H4 hysteresis loop at higher pressures that revealed the existence of slit-like mesopore [27]. From Figs. 2D and E, the Brunauer-Emmett-Teller (BET) surface areas and pore size of Fe_3O_4@UiO-66-NH_2-Zr^{4+} HFs were determined to be 243.60 m^2/g and 1.78, 8.55, 14.42 nm, respectively.

The magnetic curves of the Fe_3O_4@UiO-66-NH_2-Zr^{4+} HFs and Fe_3O_4 HFs were measured. As shown in Fig. 2F, the saturation magnetization values of Fe_3O_4@UiO-66-NH_2-Zr^{4+} HFs and Fe_3O_4 HFs were approximately 31.3 and 58.2 emu/g indicating that the surface UiO-66-NH_2-Zr^{4+} modification decreased the magnetic properties of original Fe_3O_4 HFs. To obtain detailed elemental compositions and electronic states, X-ray photoelectron spectroscopy (XPS) analysis was further carried out. From Fig. 2G, the survey spectrum of Fe_3O_4 HFs and Fe_3O_4@UiO-66-NH_2-Zr^{4+} HFs showed the presence of Fe 2p, C 1s, O 1s and Fe 2p, Zr 3d, C 1s, N 1s, O 1s elements, respectively. As seen from Fig. 2H, the binding peaks at around 182.36 and 184.72 eV were attributed to Zr $3d_{5/2}$ and Zr $3d_{3/2}$, respectively [28]. The binding energy of N 1s emission peak (Fig. 2I) observed at 398.95 and 400.62 eV, which were ascribed to the $-NH_2$ and $-NH_3^+$, respectively. Therefore, the above results obviously confirmed that the formation of Fe_3O_4@UiO-66-NH_2-Zr^{4+} HFs.

To demonstrate the feasibility of Fe_3O_4@UiO-66-NH_2-Zr^{4+} HFs as the affinity platform for enrichment of phosphopeptides, the tryptic digest of the standard phosphoprotein (β-casein) was employed as the testing sample (Fig. 3). Without any pretreatment procedure, the signals were dominated by nonphosphopeptides and only very weak signal intensity of phosphopeptide (β1s) was detected due to the low abundance and serious signal suppression by the nonphosphopeptides (Fig. 3A). Although the signals of phosphopeptide was enhanced after treatment by Fe_3O_4@UiO-66-NH_2 HFs, a number of non-phosphopeptide peaks could still be observed. Otherwise, the relatively high signal-to-noise ratio of the baseline was presented (Fig. 3B). In contrast, after enrichment with Fe_3O_4@UiO-66-NH_2-Zr^{4+} HFs, strong signals of phosphopeptide dominated the spectrum and the clean mass spectrometry (MS) background was obtained (Fig. 3C). In addition, three phosphopeptides (β1s, β2s and β3m) and their dephosphopeptide

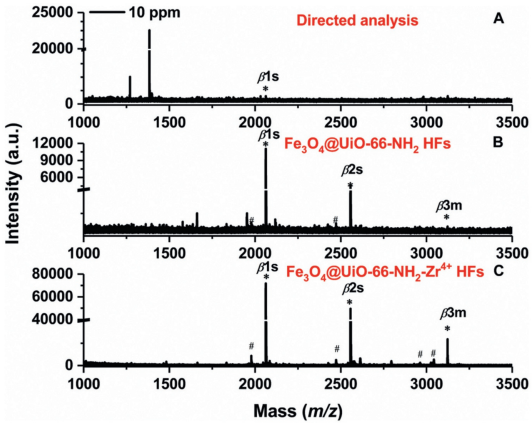

Fig. 3. MALDI-TOF mass spectra of the tryptic digests of β-casein: direct analysis (A), analysis after enrichment with Fe_3O_4@UiO-66-NH_2 HFs (B), analysis after enrichment with Fe_3O_4@UiO-66-NH_2-Zr^{4+} HFs (C). "*" and "#" indicate phosphorylated peptides and their dephosphorylated counterparts, respectively.

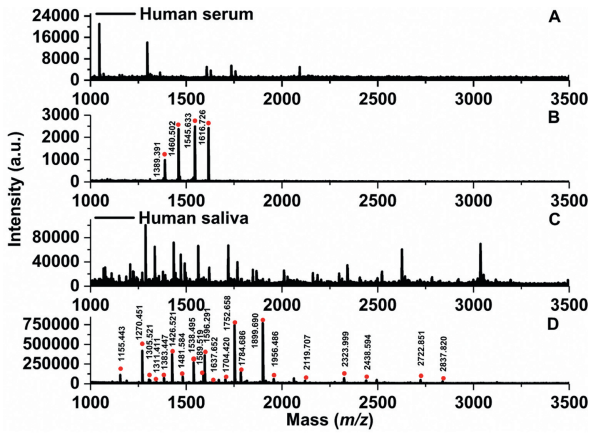

Fig. 4. MALDI-TOF mass spectra of the tryptic digests of human serum and saliva: Direct analysis (A, C) and analysis after enrichment by the Fe_3O_4@UiO-66-NH_2-Zr^{4+} HFs (B, D).

were all detected with strong signals. The details of the phosphopeptides were listed in Table S1 (Supporting information).

To prove that hollow nanoflower structure helped to improve extraction performance, the extraction capacity of Fe_3O_4@UiO-66-NH_2-Zr^{4+} HFs and Fe_3O_4@UiO-66-NH_2-Zr^{4+} NPs for phosphopeptides were compared under the same conditions. From Fig. S2 (Supporting information), after enrichment with Fe_3O_4@UiO-66-NH_2-Zr^{4+} HFs, the intensity of the three characteristic signal peaks of the phosphopeptide (β1s, β2s, β3m) were all much higher than that after enrichment with Fe_3O_4@UiO-66-NH_2-Zr^{4+} NPs. Fe_3O_4@UiO-66-NH_2-Zr^{4+} HFs showed better enrichment performance might be attributed to the following reasons. Firstly, the hierarchical pores of the special nanoflower structure could more freely allow targets to enter the surface and cavity, providing more accessible sites. Simultaneously, the hollow structure made the active sites inside the material more accessible, ensuring the material properties was used to the greatest extent. Finally, the cavity could hold more targets, accompanied by an increase in adsorption efficiency [29]. The conclusion was summarized that the unique shape of hollow nanoflowers played a crucial role in the selective enrichment of phosphopeptides.

To investigate selectivity of Fe_3O_4@UiO-66-NH_2-Zr^{4+} HFs toward phosphopeptides, the tryptic digest mixture of β-casein and bovine serum albumin (BSA) at different molar ratios (1:1000) were used as imitative biological sample. Before enrichment, abundant nonphosphopeptides peaks dominated the chromatogram accompanying with relatively high baseline signal. No any peaks of phosphopeptides were detected, which could be caused by the MS signals of phosphopeptides in the mixture solution (β-casein:BSA=1:1000) were seriously suppressed by the nonphosphopeptides from BSA digest (Fig. S3A in Supporting information). However, after treatment with Fe_3O_4@UiO-66-NH_2-Zr^{4+} HFs, three phosphopeptides (m/z = 2061.9, 2566.9 and 3122.6) with high intensities and a relatively clear background were achieved (Fig. S3B in Supporting information), which was better than previously reported materials of MCNC@COF@Zr^{4+} (1:200) [30], mSiO_2@PEI (1:100) [31], SiO_2@ATP-Ti^{4+} (1:1) [32], Fe_3O_4@C-phosphate-Zr^{4+} (1:25) [33], and Fe_3O_4@nSiO_2@mSiO_2/TiO_2-Ti^{4+} (1:50) [34]. The results indicated the high selectivity of Fe_3O_4@UiO-66-NH_2-Zr^{4+} HFs as affinity platform for enrichment of phosphopeptides.

Considering the special hollow nanoflower structure of material, it was expected that Fe_3O_4@UiO-66-NH_2-Zr^{4+} HFs could exclude the large-size interfering substances in the enrichment of phosphopeptides from complex mixture. To test size-exclusion effect, the β-casein digest was mixed with BSA directly at a molar ratio of 1:200 was chosen as a model sample. From Fig. S4C (Supporting information), BSA protein was obviously observed in high molecular weight region without enrichment, while no phosphopeptides could be detected in the low molecular weight region and abundant nonphosphopeptides peaks dominated the chromatogram (Fig. S4A in Supporting information). On the contrary, after treatment by Fe_3O_4@UiO-66-NH_2-Zr^{4+} HFs, three phosphopeptides with strong intensity were identified (Fig. S4B in Supporting information) and no signal of BSA protein was observed (Fig. S4D in Supporting information). The result indicated that the affinity of Fe_3O_4@UiO-66-NH_2-Zr^{4+} HFs toward small-size phosphopeptides would be not affected by the large proteins, indicating its potential application in complex biosamples.

To further explore the sensitivity of the proposed method for the enrichment of phosphopeptides, tryptic digests of β-casein with different concentrations were investigated based on the Fe_3O_4@UiO-66-NH_2-Zr^{4+} HFs (Fig. S5 in Supporting information). Three phosphopeptides were still clearly detected with a relatively high signal (signal-to-noise ratio $>$ 3) even at the concentration as low as 10 fmol (Fig. S5B). Surprisingly, one phosphopeptide peak (β1s) could still be identified when the concentration was as low as 1 fmol (Fig. S5C). The result showed that the prepared material exhibited the better performance than previously reported [30,35-37]. Undoubtedly, Fe_3O_4@UiO-66-NH_2-Zr^{4+} HFs had good affinity for phosphopeptides.

Encouraged by all achieved results, Fe_3O_4@UiO-66-NH_2-Zr^{4+} HFs were further applied to capture endogenous phosphopeptide in complex biosamples of human saliva and serum. we had obtained an approval from the Ethics Committee of Biomedical Scientific Research Henan University (HUSOM2024-394). As a widely used clinical sample, human saliva and serum were easy to get and contained many low-abundance endogenous phosphopeptides which could be the potential biomarkers for disease diagnosis. For human serum, without enrichment, nonphosphopeptides dominated the spectrum and no any signal of phosphopeptide could be detected, indicating the interferences were quite seriously (Fig. 4A). On the contrary, after enrichment with Fe_3O_4@UiO-66-NH_2-Zr^{4+} HFs, four phosphopeptides were clearly detected with high intensity (Fig. 4B) and the detailed information of the captured phosphopeptides were listed in Table S2 (Supporting information). For human saliva, before enrichment, also no any phosphopeptide signal was detected, and severe signal suppression with high baseline were found (Fig. 4C). Obviously, after enrichment, 21 endogenous

phosphopeptides were detected accompanying the clean baseline signal (Fig. 4D). All peaks were consistent with those reported in the literature [30,38-40]. The enrichment results indicated that the Fe_3O_4@UiO-66-NH_2-Zr^{4+} HFs could be used as enriched material to capture endogenous phosphopeptides from real biological samples with high efficiency.

A general strategy for thickness-controllable synthesis of MOF-based heterogeneous material with special hollow nanoflowers shapes was demonstrated. The thickness could be freely controlled by changing the assembly cycles. The as-prepared MOF-based heterogeneous material possessed the unique hollow nanoflower structure, well-defined hierarchical pores, good superparamagnetic property, large surface area and good hydrophilicity. Furthermore, after post-modification with Zr^{4+}, the Fe_3O_4@UiO-66-NH_2-Zr^{4+} HFs showed the ability to selective enrichment of phosphopeptide accompanying with high selectivity, sensitivity and excellent size-exclusion effect. In addition, the Fe_3O_4@UiO-66-NH_2-Zr^{4+} HFs were successfully applied to specific capture of ultratrace phosphopeptide from complex biosamples. This work will provide a new route for thickness-controllable synthesis of MOF-based heterogeneous material with special hollow nanoflowers shapes, and also shows promising potential in clinical analysis.

Declaration of competing interest

The authors declare no competing interests.

CRediT authorship contribution statement

Ning Zhang: Conceptualization, Writing – original draft. **Mengjie Qin:** Data curation. **Jiawen Zhu:** Investigation, Methodology. **Xuejing Lou:** Formal analysis, Investigation. **Xiao Tian:** Data curation, Methodology. **Wende Ma:** Funding acquisition, Software. **Youmei Wang:** Validation, Visualization. **Minghua Lu:** Funding acquisition, Project administration, Writing – review & editing. **Zongwei Cai:** Writing – review & editing.

Acknowledgments

This work was sponsored by the National Natural Science Foundation of China (Nos. 22106038, 22204171 and 22076038), the Henan Provincial Science and Technology Research Project (No. 232102310112), the China Postdoctoral Science Foundation (No. 2022M713299), Natural Science Foundation of Henan Province, China (No. 202300410044), Henan key scientific research programs to Universities and Colleges (No. 22ZX003).

Supplementary materials

Supplementary material associated with this article can be found, in the online version, at doi:10.1016/j.cclet.2024.110177.

References

[1] Y.J. Zhang, P.M. Radjenovic, X.S. Zhou, et al., Adv. Mater. 33 (2021) 2005900.
[2] Y. Liu, Y. Yang, Y.J. Sun, et al., J. Am. Chem. Soc. 141 (2019) 7407–7413.
[3] P.X. Liu, Y. Zhao, R.X. Qin, et al., Science 352 (2016) 797–802.
[4] Y. Chen, D. Yang, B.B. Shi, et al., J. Mater. Chem. A 8 (2020) 7724–7732.
[5] M.J. Sailor, J. Park, Adv. Mater. 24 (2012) 3779–3802.
[6] R.K. Nutor, Q.P. Cao, R. Wei, et al., Sci. Adv. 7 (2021) 4404.
[7] C.A. Witham, W. Huang, C.K. Tsung, et al., Nat. Chem. 2 (2010) 36–41.
[8] S. Schauermann, N. Nilius, S. Shaikhutdinov, H.J. Freund, Acc. Chem. Res. 46 (2013) 1673–1681.
[9] B.L. Xue, X.W. Geng, H.H. Cui, et al., Chin. Chem. Lett. 34 (2023) 108140.
[10] L.Y. Chen, M. Rong, J.M. Yu, et al., Chem. Eng. J. 457 (2023) 141326.
[11] Z.X. Xu, H.L. Chen, H.M. Chu, et al., Chin. Chem. Lett. 34 (2023) 107829.
[12] H. Liu, Q.Q. Li, P.H. Pan, et al., Chin. Chem. Lett. 34 (2023) 108562.
[13] M.Z. Hu, S. Zhao, S.J. Liu, et al., Adv. Mater. 30 (2018) 1801878.
[14] J. Yang, F.J. Zhang, X. Wang, et al., Angew. Chem. Int. Ed. 55 (2016) 12854–12858.
[15] W. Huang, Q. He, Y.P. Hu, Y.G. Li, Angew. Chem. Int. Ed. 58 (2019) 8676–8680.
[16] Z.N. Wang, M.Y. Liu, F. Xiao, Chin. Chem. Lett. 33 (2022) 653–662.
[17] H.M. Chu, H.Y. Zheng, A.Z. Miao, C.H. Deng, N.R. Sun, Chin. Chem. Lett. 34 (2023) 107716.
[18] N.R. Sun, H.L. Yu, Hao Wu, X.Z. Shen, C.H. Deng, TrAC, Trends Anal. Chem. 135 (2021) 116168.
[19] Y.X. Sun, K.J. Quan, J. Chen, et al., Chin. Chem. Lett. 34 (2023) 108166.
[20] Z. Zhang, W. Yu, J. Wang, et al., Anal. Chem. 89 (2017) 1416–1420.
[21] C.Y. Tsai, C.H. Chang, T.L. Kao, K.T. Chen, H.Y. Tuan, Chem. Eng. J. 417 (2021) 128552.
[22] L. Cao, P.C. Dai, J. Tang, et al., J. Am. Chem. Soc. 142 (2020) 8755–8762.
[23] R. Wang, H. Qi, H.J. Zheng, Q. Jia, Chin. Chem. Lett. 35 (2024) 109215.
[24] J.N. Zheng, Z.A. Lin, L. Zhang, H.H. Yang, Sci. China Chem. 58 (2015) 1056–1064.
[25] P.C. Lemaire, D.T. Lee, J.J. Zhao, G.N. Parsons, ACS Appl. Mater. Interfaces 9 (2017) 22042–22054.
[26] J.M. Wei, W. Zhang, W.Y. Pan, C.R. Li, W.L. Sun, Environ. Sci. Nano. 5 (2018) 1441–1453.
[27] Y.F. Shen, Y.W. Zhou, Y.H. Fu, N.Y. Zhang, Renew. Energ. 146 (2020) 1700–1709.
[28] L.J. Shen, W.M. Wu, R.W. Liang, R. Lin, L. Wu, Nanoscale 5 (2013) 9374–9382.
[29] J. Yang, F.J. Zhang, H.Y. Lu, et al., Angew. Chem. Int. Ed. 54 (2015) 10889–10893.
[30] C.H. Gao, J. Bai, Y.T. He, et al., ACS Appl. Mater. Interfaces 11 (2019) 13735–13741.
[31] G.T. Zhu, X.M. He, S. He, et al., ACS Appl. Mater. Interfaces 8 (2016) 32182–32188.
[32] H. Wang, Z.X. Tian, J. Chromatogr. A 1564 (2018) 69–75.
[33] D.W. Qi, Y. Mao, J. Lu, C.H. Deng, X.M. Zhang, J. Chromatogr. A 1217 (2010) 2606–2617.
[34] D.S. Yang, X.Y. Ding, H.P. Min, et al., J. Chromatogr. A 1505 (2017) 56–62.
[35] H.M. Chu, H.Y. Zheng, N.R. Sun, C.H. Deng, Anal. Chim. Acta 1195 (2022) 338693.
[36] B.D. Zhu, Q. Zhou, D.S. Zhen, et al., Talanta 194 (2019) 870–875.
[37] J.Y. Dai, M.D. Wang, H.L. Liu, Talanta 164 (2017) 222–227.
[38] H.Z. Lin, H.M. Chen, X. Shao, C.H. Deng, Microchim. Acta 185 (2018) 562.
[39] J. Su, X.W. He, L.X. Chen, Y.K. Zhang, ACS Sustain. Chem. Eng. 6 (2018) 2188–2196.
[40] J.W. Wang, Z.D. Wang, N.R. Sun, C.H. Deng, Microchim. Acta 186 (2019) 236.